Therapeutic lymphangiogenesis ameliorates established acute lung allograft rejection

Ye Cui,[1] Kaifeng Liu,[2] Maria E. Monzon-Medina,[3] Robert F. Padera,[4] Hao Wang,[1] Gautam George,[1] Demet Toprak,[2] Elie Abdelnour,[1] Emmanuel D'Agostino,[1] Hilary J. Goldberg,[1] Mark A. Perrella,[1,5] Rosanna Malbran Forteza,[3] Ivan O. Rosas,[1] Gary Visner,[2] and Souheil El-Chemaly[1]

[1]Division of Pulmonary and Critical Care Medicine, Brigham and Women's Hospital, Harvard Medical School, Boston, Massachusetts, USA. [2]Department of Pediatrics, Boston Children's Hospital, Harvard Medical School, Boston, Massachusetts, USA. [3]Division of Pulmonary Critical Care, Sleep and Allergy Medicine, University of Miami Miller School of Medicine, Miami, Florida, USA. [4]Department of Pathology and [5]Department of Pediatric Newborn Medicine, Brigham and Women's Hospital, Harvard Medical School, Boston, Massachusetts, USA.

Lung transplantation is the only viable option for patients suffering from otherwise incurable end-stage pulmonary diseases such as chronic obstructive pulmonary disease and idiopathic pulmonary fibrosis. Despite aggressive immunosuppression, acute rejection of the lung allograft occurs in over half of transplant recipients, and the factors that promote lung acceptance are poorly understood. The contribution of lymphatic vessels to transplant pathophysiology remains controversial, and data that directly address the exact roles of lymphatic vessels in lung allograft function and survival are limited. Here, we have shown that there is a marked decline in the density of lymphatic vessels, accompanied by accumulation of low-MW hyaluronan (HA) in mouse orthotopic allografts undergoing rejection. We found that stimulation of lymphangiogenesis with VEGF-C156S, a mutant form of VEGF-C with selective VEGFR-3 binding, alleviates an established rejection response and improves clearance of HA from the lung allograft. Longitudinal analysis of transbronchial biopsies from human lung transplant recipients demonstrated an association between resolution of acute lung rejection and decreased HA in the graft tissue. Taken together, these results indicate that lymphatic vessel formation after lung transplantation mediates HA drainage and suggest that treatments to stimulate lymphangiogenesis have promise for improving graft outcomes.

Introduction

Lung transplantation remains the optimal treatment to prolong survival and improve quality of life for patients with end-stage lung disease (1). While outcomes after lung transplantation continue to improve, the 5-year survival rate is still far below the rates achieved following other solid organ transplantations (2). Despite aggressive immunosuppressive treatments, acute rejection occurs in up to 55% of lung allograft recipients and is one of the leading causes of morbidity during the first year after transplantation (3, 4). In addition, recurrent acute rejection represents a primary risk factor for the development of bronchiolitis obliterans syndrome (BOS), or chronic allograft rejection, which is a major impediment to long-term survival (5–8). Since the efficacy of immunosuppression is less than ideal, continued exploration of novel therapeutic options is imperative.

Lung transplantation involves airway, arterial, and venous connections at the time of surgery (9). Notably, anastomosis of severed donor lymphatic vessels to those of the recipient is not performed due to technical challenges, resulting in complete interruption of lymphatic drainage. Reestablishment of a lymphatic continuum after transplantation relies on formation of new lymphatic vessels (lymphangiogenesis), the exact roles of which remain enigmatic and somewhat controversial in transplant pathophysiology (10, 11). While some studies have shown a beneficial role of lymphatic vessels in transplantation (12–15), the prevailing view holds that they contribute to alloimmune responses that will result in the exacerbation of allograft rejection (16–19). Therefore, it has been suggested that inhibiting lymphangiogenesis could be critical for graft tolerance and survival (20, 21). However, lung allografts are acutely rejected within 7 days after transplantation in animal transplant models (22–25), whereas spontaneous restoration of lymphatic drainage from the transplanted lung to the lymph nodes occurs no earlier than day 7 after transplantation (26, 27). Since the onset of lung rejection precedes the reestablishment of lymphatic continuity, it is possible that insufficient lymphatic drainage could be responsible, at least in part, for acute lung allograft rejection.

Hyaluronan (HA) is a ubiquitously distributed extracellular matrix glycosaminoglycan that exists physiologically as a high-MW (HMW) polymer but undergoes extensive fragmentation in response to tissue injury (28–31). HA has been previously associated with lung injury and repair through multiple pathways driven by HA receptors such as CD44 and TLR2 and TLR4 (29, 31, 32). More recently, low-MW HA was shown to play important roles in the development of BOS through TLR2/4-dependent pathways, leading to increased numbers of neutrophils and alloantigen-specific T lymphocytes, while HMW HA decreased graft inflammation (33). Increased HA content and fragmentation contribute

▶ Related Commentary: p. 3999

Conflict of interest: The authors have declared that no conflict of interest exists.
Submitted: November 11, 2014; **Accepted:** August 28, 2015.
Reference information: *J Clin Invest*. 2015;125(11):4255–4268. doi:10.1172/JCI79693.

to transplant rejection (32–34), although it is unclear whether the abundant presence of HA also reflects a lack of its effective drainage in rejected allografts. Since the turnover of HA (several grams/day in humans) occurs primarily through lymphatics (approximately 85%) (35, 36), where uptake is mediated by the lymphatic vessel endothelial HA receptor LYVE-1, we hypothesized that HA clearance impairment due to severely compromised lymphatic drainage might lead to its aberrant accumulation in lungs undergoing rejection. To test this hypothesis, we performed gain-of-function (therapeutically inducing lymphangiogenesis to promote HA drainage) as well as loss-of-function (blocking HA uptake by lymphatic endothelial cells [LECs]) experiments in a mouse model of orthotopic lung transplantation. In addition, we analyzed sequential transbronchial biopsy (TBB) specimens from human lung transplant recipients to determine whether the observations made in the mouse model are consistent with clinical events.

Results

Acute lung allograft rejection leads to loss of lymphatic vessels. To assess the fate of lymphatic vessels in lung transplants, we first performed mouse orthotopic left lung transplantation using the 3-cuff technique for vascular and airway anastomoses (Figure 1, A and B), as previously described (37, 38). We sacrificed the animals 30 days after transplantation and visualized the lymphatic vessels using antibodies against LYVE-1, a widely used marker of LECs (39–41). Consistent with previous observations (22, 23), the histological appearance of mouse left lung isografts (C57BL/6 donor to C57BL/6 recipient) was comparable to that of untransplanted lungs of age-matched normal controls (Figure 1C and Supplemental Figure 1A; supplemental material available online with this article; doi:10.1172/JCI79693DS1). As expected, allograft lungs (BALB/c donor to fully MHC-mismatched C57BL/6 recipient) displayed histopathological features of severe acute rejection, with prominent perivascular and interstitial mononuclear cell infiltrates. In lung tissues from normal mice and isografts, vascular structures expressing LYVE-1 were distributed throughout the lung parenchyma (Figure 1D, left panel, and Supplemental Figure 1B). In contrast, we noticed a diminished presence of lymphatic vessels in allografts undergoing rejection. To quantitatively evaluate lymphatic vessel density, we counted the total number of LYVE-1–positive lymphatic vessels in the section and adjusted it to the cross-sectional area of the entire tissue (Supplemental Figure 2). Our results showed that there was a marked decline in the density of LYVE-1–positive lymphatic vessels in lung allografts compared with control lungs and isografts (Figure 1D, right panel). Since LYVE-1 expression is largely but not exclusively restricted to lymphatic vessels (42, 43), we performed double immunofluorescence staining using antibodies against VEGFR-3 and PROX-1 (markers of LECs). As shown in Figure 1E and Supplemental Figure 3A, results from VEGFR-3/PROX-1 double immunostaining confirmed the decrease in lymphatic vessel density in acute allograft rejection (Figure 1E, right panel). Additionally, quantitative analysis did not reveal a significant difference in the percentage of VEGFR-3–positive lymphatic vessels with PROX-1–positive nuclei or in the percentage of PROX-1/VEGFR-3–double-positive cells in the identified lymphatic vessels among the experimental groups (Supplemental Figure 3, B and C).

Treatment with VEGF-C156S attenuates established allograft lung rejection and is associated with improved HA clearance. Given these findings, we sought to determine the effects of VEGF-C156S–induced lymphangiogenesis on lung allograft function. VEGF-C156S, a VEGF-C mutant with exclusive binding affinity for VEGFR-3, induces lymphangiogenesis but not angiogenesis (44–47). VEGF-C156S was administered to animals through daily i.v. injections after the onset of acute allograft rejection (days 20 to 30 after transplantation). Considering that lymphatic vessels facilitate the uptake of HA fragments through the transmembrane receptor LYVE-1 in LECs (48, 49) and that increased levels of HA are associated with allograft rejection (32–34), we further explored the exact roles of lymphatic vessels in transplant pathophysiology through a parallel loss-of-function experiment, in which a group of VEGF-C156S–treated allograft recipients were simultaneously treated with LYVE-1 function–blocking antibodies via i.p. injection (ref. 50 and Supplemental Figure 4). Vehicle-treated (PBS-treated) lung allografts were visibly shrunken and discolored compared with the control lungs, whereas VEGF-C156S–treated allografts exhibited noticeably fewer signs of injury (Figure 2A). Remarkably, however, concomitant neutralization of LYVE-1 function abrogated the therapeutic benefits of VEGF-C156S, as evidenced by the dark red and mottled appearance of allografts. In accordance with gross observations, microscopic evaluation revealed that VEGF-C156S alone led to partial amelioration of graft rejection, indicated by a significant reduction in the acute cellular rejection (ACR) score, whereas blocking LYVE-1 cell-surface receptors largely reversed the histological improvement associated with VEGF-C156S (Figure 2B and Supplemental Figure 5A). Consistent with its known role as a selective agonist of VEGFR-3 (44–46, 51), VEGF-C156S treatment resulted in the induction of lymphangiogenesis in transplanted left lungs (Figure 2, C and D, Supplemental Figure 5B, and Supplemental Figure 6A), but had no effect on blood vessel density (Supplemental Figure 7). Furthermore, the percentage of VEGFR-3–positive lymphatic vessels with PROX-1–positive nuclei was comparable across all groups (Supplemental Figure 6B), and there was no significant difference in the percentage of cells double-positive for VEGFR-3/PROX-1 in the identified lymphatic vessels (Supplemental Figure 6C).

Visualization of HA distribution was achieved using biotinylated HA–binding protein (HABP), and its labeling specificity was subsequently confirmed by pretreatment with hyaluronidase (Supplemental Figure 8). In control lungs, HABP staining was predominantly observed in the connective tissues around bronchi, bronchioles, and blood vessels (Figure 2E and Supplemental Figure 5C). In PBS-treated allografts, the area of HABP staining expanded evidently beyond the peribronchial and perivascular regions, and there was substantial accumulation of HA in both the alveolar airspace and interstitium. In response to VEGF-C156S treatment, the amount of HA in lung parenchyma of the allografts was dramatically reduced, yet simultaneously blocking LYVE-1 aggravated HA deposition, suggesting that decreased clearance of HA was involved in lung rejection.

In order to characterize HA during rejection, we estimated its size by agarose gel electrophoresis. We found that there was a downward shift in HA molecular mass in PBS-treated allografts

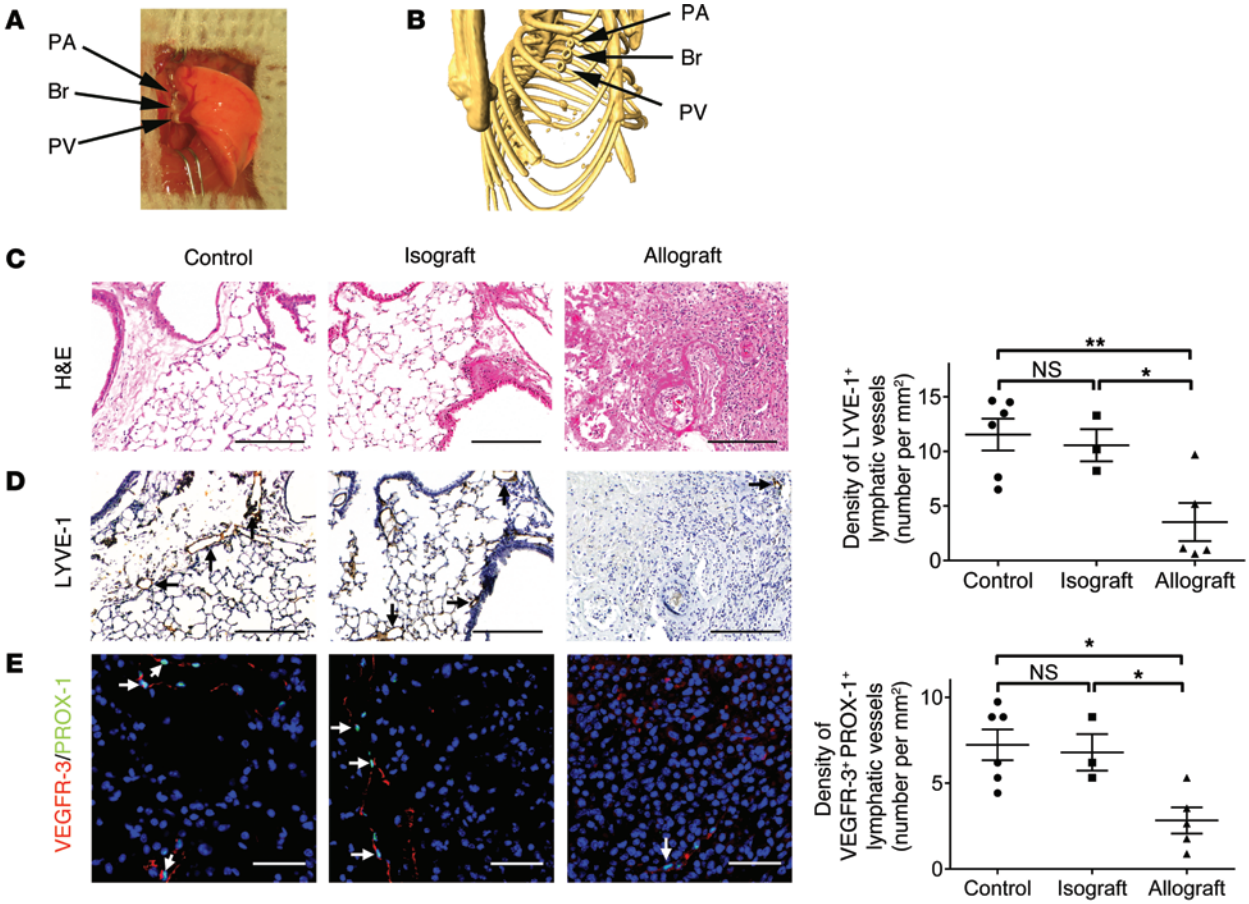

Figure 1. Decreased lymphatic vessel density in lung allograft rejection. (**A**) Gross appearance of mouse orthotopic left lung transplant using the 3-cuff technique. (**B**) Reconstituted 3D μCT of the bronchial and vascular cuffs on day 30 after transplantation. (**C**) Representative images of H&E-stained sections. (**D**) Representative images of LYVE-1 immunohistochemical staining (LYVE-1–positive lymphatic vessels are indicated by black arrows, left panel) and quantification of LYVE-1–positive lymphatic vessel density (right panel). (**E**) Left panel: representative images of PROX-1 (green)/VEGFR-3 (red) double immunofluorescence staining. PROX-1/VEGFR-3–double-positive cells are indicated by white arrows. Nuclei were counterstained with DAPI (blue). Right panel: quantification of PROX-1/VEGFR-3–double-positive lymphatic vessel density. Scale bars: 200 μm (**C** and **D**); 50 μm (**E**). Animals receiving isogeneic (n = 3 mice) or allogeneic (n = 5 mice) lung grafts were sacrificed 30 days after transplantation, together with age-matched untransplanted controls (n = 6 mice). Data are presented as the mean ± SEM. *$P < 0.05$, **$P < 0.01$, as determined by 1-way ANOVA. PA, pulmonary artery; Br, bronchus; PV, pulmonary vein.

compared with that detected in control lungs, whereas the range of HA molecular mass in VEGF-C156S–treated allografts was commensurate with that of the native form. By contrast, treatment with LYVE-1 function–blocking antibodies resulted in a pronounced retention of fragmented HA (Figure 3). Collectively, these findings show that impaired lymphatic transport coincides with the persistence of allograft rejection, which depends, at least in part, on the aberrant accumulation of HA fragments in the lung.

While the majority of experimental studies use localized administration of prolymphangiogenic growth therapy (45, 52), recent reports demonstrated that systemic delivery of prolymphangiogenic growth factors could also promote lymphangiogenesis in distant organs (51, 53). To further confirm the efficacy of VEGF-C156S i.v. injection, we evaluated lymphatic vessels and HA in nontransplanted right lungs. Quantification of VEGF-R3/PROX-1 double immunostaining showed that similar to the left lungs, there was increased lymphangiogenesis in the native lungs with systemic administration of VEGF-C156S (Supplemental Figure 9A). Interestingly, HA deposition (Supplemental Figure 9B) and molecular mass (Supplemental Figure 10) were not affected by either VEGF-C156S treatment or concomitant LYVE-1 blocking.

Treatment with VEGF-C156S decreases LEC apoptosis and increases LEC proliferation. Since apoptosis contributes to significant cell loss in lung transplantation (54, 55), we hypothesized that the diminished presence of pulmonary lymphatic vessels in rejected allografts might be associated with increased apoptosis of lung LECs. To this end, we conducted double immunofluorescence labeling with TUNEL and anti–PROX-1 antibodies in mouse lung tissue. Quantification of images acquired using confocal microscopy did not reveal a significant difference in the percentage of apoptotic LECs between control lungs and isografts. In contrast, the proportion of apoptotic LECs increased by approximately 4-fold in PBS-treated allografts compared with the numbers observed in control lungs, yet this increase was reduced by more than half in allografts treated with VEGF-C156S (Figure 4A and Supplemental Figure 11). Considering that the change in lymphatic density could also represent a net effect of altered LEC apoptosis and proliferation, we examined whether LEC proliferation was affected in var-

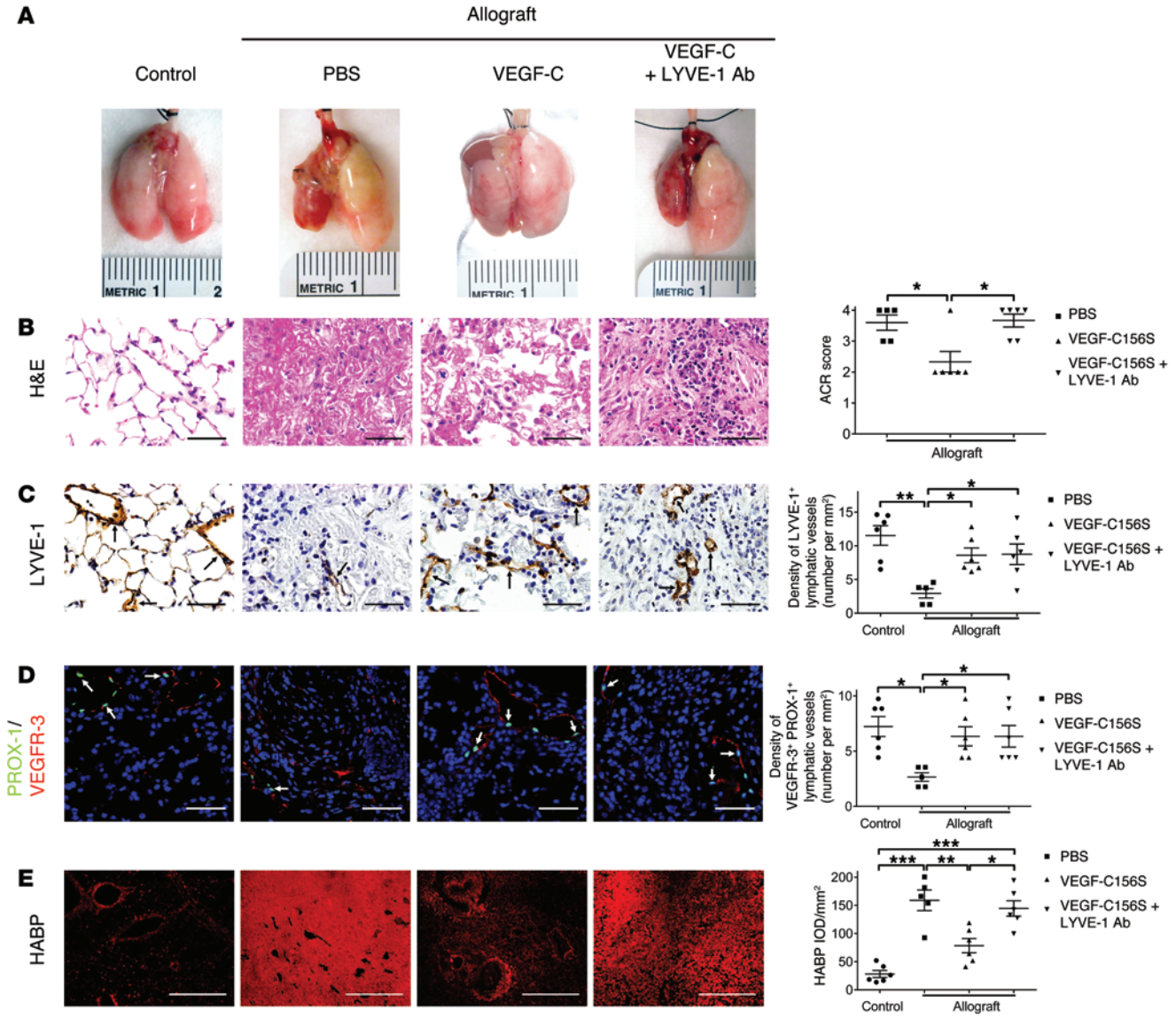

Figure 2. VEGF-C156S treatment attenuates lung allograft rejection by clearing HA. (**A**) Representative gross appearance of control untransplanted lungs and allografts treated with PBS or VEGF-C156S (VEGF-C) or concomitantly treated with VEGF-C156S and LYVE-1 function–blocking antibodies (VEGF-C + LYVE-1 Ab). Transplanted grafts are depicted on the left side. (**B**) Representative images of H&E-stained sections (left panel) and ACR scores (right panel). (**C**) Representative images of LYVE-1 immunohistochemical staining (LYVE-1–positive lymphatic vessels are indicated by black arrows, left panel) and quantification of LYVE-1–positive lymphatic vessel density (right panel). (**D**) Left panel: representative images of PROX-1 (green)/VEGFR-3 (red) double immunofluorescence staining. PROX-1/VEGFR-3–double-positive cells are indicated by white arrows. Nuclei were counterstained with DAPI (blue). Right panel: quantification of PROX-1/VEGFR-3–double-positive lymphatic vessel density. (**E**) Representative images of HABP fluorescent staining (red, left panel) and quantification of HABP IOD (right panel). Scale bars: 50 μm (**B**–**D**); 500 μm (**E**). Animals receiving allogeneic lung grafts were treated with PBS (n = 5) or VEGF-C156S (n = 6) or were concomitantly treated with VEGF-C156S and LYVE-1 function–blocking antibody (n = 6) from days 20 to 30 after transplantation. Age-matched untransplanted animals were used as controls (n = 6). All data are presented as the mean ± SEM. $^{*}P < 0.05$, $^{**}P < 0.01$, $^{***}P < 0.001$, as determined by 1-way ANOVA.

ious experimental conditions using double immunostaining with PROX-1 and proliferating cell nuclear antigen (PCNA), a marker of cell proliferation. We observed that increased LEC apoptosis in PBS-treated allografts was accompanied by a significant decrease in the ratio of LECs expressing PCNA (Figure 4B and Supplemental Figure 12). Furthermore, consistent with previous findings (56, 57), we showed that VEGF-C156S treatment resulted in an approximately 5-fold increase in LEC proliferation compared with that seen in PBS-treated allografts.

VEGF-C156S treatment reduces inflammatory cell infiltration into allografts. Recruitment of inflammatory cells is an essential step leading to allograft rejection (4). In order to examine the effects of VEGF-C156S on inflammatory cell infiltration into allografts, we performed IHC staining for T cells and macrophages using anti-CD3 and anti-CD68 antibodies, respectively (Figure 5, A and B). Inflammatory cell infiltrates were rarely detected in control lungs, whereas allografts treated with PBS were characterized by a marked increase in the number of both T cells and

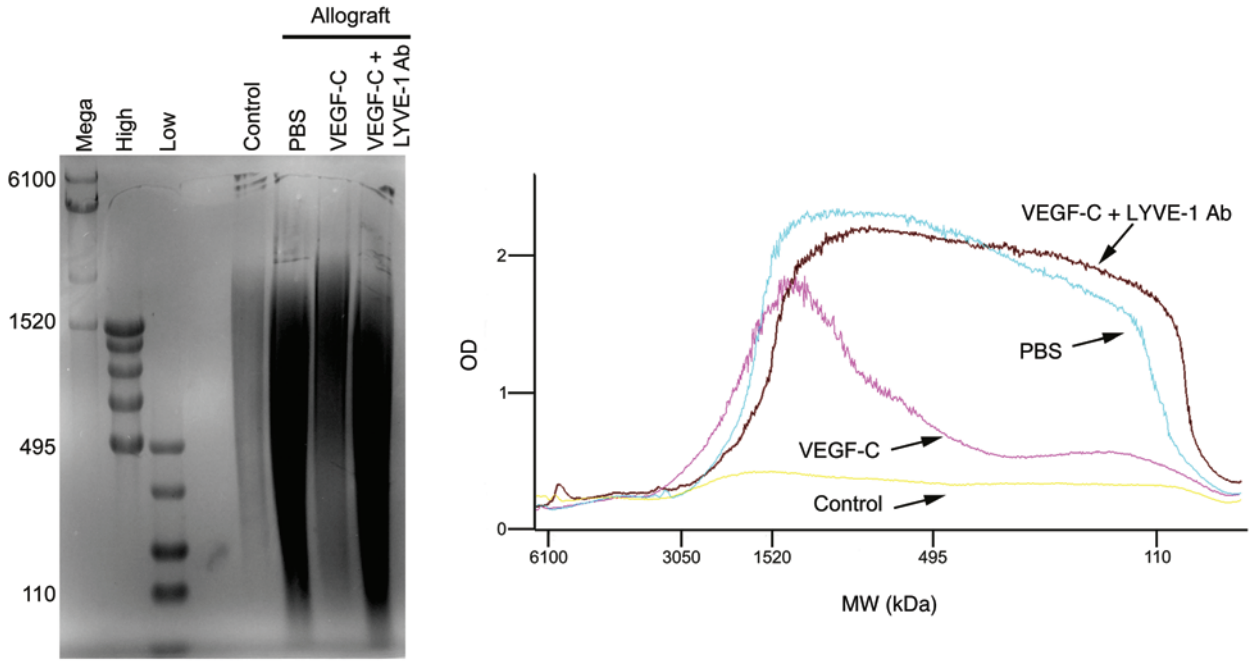

Figure 3. VEGF-C156S treatment inhibits the downward shift of HA molecular mass in lung allograft rejection. Left panel: agarose gel electrophoresis was conducted to analyze HA size in mouse left lungs. From left to right: mega (6100, 4570, 3050, and 1520 kDa), high (1510, 1090, 966, 572, and 495 kDa), and low (495, 310, 214, 110, and 27 kDa) HA ladders were used to determine the molecular mass of HA in tissue samples. HA samples per lane were pooled from the upper portions of mouse left lungs in each group. Right panel: quantitative analysis of HA profiles in mouse left lungs. Animals receiving allogeneic left lung grafts were treated with PBS (n = 5 mice) or VEGF-C156S (VEGF-C) (n = 6 mice) or were concomitantly treated with VEGF-C156S and LYVE-1 function–blocking antibody (VEGF-C + LYVE-1 Ab) (n = 6 mice) from day 20 to day 30 after transplantation. Age-matched untransplanted animals were used as controls (n = 6 mice).

macrophages. Following VEGF-C156S treatment, there was a substantial decline in the number of CD3- and CD68-positive cells in the allografts. However, concomitantly blocking LYVE-1 resulted in extensive infiltration of T cells and macrophages to levels that were comparable to those found in PBS-treated allografts.

Several reports have identified that a subset of macrophages express LYVE-1 (58–60). Therefore, it is possible that LYVE-1–positive macrophages might play a role in HA clearance and potentially contribute to the resolution of allograft rejection. To assess the presence of LYVE-1–positive macrophages in allografts, we performed double immunofluorescence staining with anti-CD68 and anti–LYVE-1 antibodies (Figure 5C, left panel). Double-positive cells were scarcely detected in control lungs, but were more prevalent in PBS-treated allografts. On the other hand, VEGF-C156S treatment reduced the amount of LYVE-1–positive macrophages in allografts by approximately two-thirds, yet simultaneous LYVE-1 blocking largely reversed this trend to a level similar to that observed in PBS-treated allografts (Figure 5C, upper-right panel). Further quantification also revealed that the proportions of CD68/LYVE-1–double-positive cells were elevated to similar levels in all the experimental groups with allograft transplants (Figure 5C, lower-right panel).

VEGF-C156S treatment restores a functional lymphatic continuum in lung allografts. Lymphatic continuity is inevitably disrupted during lung transplantation surgery. Since VEGF-C156S treatment has been shown to reestablish damaged lymphatic transport in an incision wound model (61), we sought to determine whether such treatment could also affect severed lymphatic vessels in mouse lung allografts. For this purpose, we performed a pulmonary dextran–Alexa Fluor 488 (488-dextran) drainage assay (50) in control and transplanted mice to evaluate lymphatic transport from left lungs to their draining lymph nodes. In control mice, green fluorescence was visualized in tracheobronchial lymph nodes 50 minutes after unilateral instillation of 488-dextran solution into mouse left lungs (Figure 6). By 20 days after transplantation, mouse left lungs showed more than a 4-fold increase in 488-dextran integrated optical density (IOD) in allografts compared with that in isografts. This was accompanied by the presence of 488-dextran in the tracheobronchial lymph nodes of isograft but not allograft recipients. The fluorescent signal remained absent in the draining lymph nodes of PBS-treated animals by day 30 after transplantation. Remarkably, however, compared with PBS-treated animals, VEGF-C156S treatment resulted in a nearly 50% decrease in 488-dextran IOD, with detectable drainage into the tracheobronchial lymph nodes, indicating a recovery of lymphatic function.

VEGF-C156S treatment improves radiographic and pulmonary function parameters in acute allograft lung rejection. In order to longitudinally monitor the changes in lung allografts from individual mice, we performed micro-CT (μCT) scanning before and after the experimental interventions. Compared with healthy lungs, axial slides from allografts on day 20 after transplantation (prior to treatment) revealed a dense, homogenous opacity occupying the entire left lung field (Figure 7A). The μCT findings from axial and reconstituted 3D images from PBS-treated allografts on day

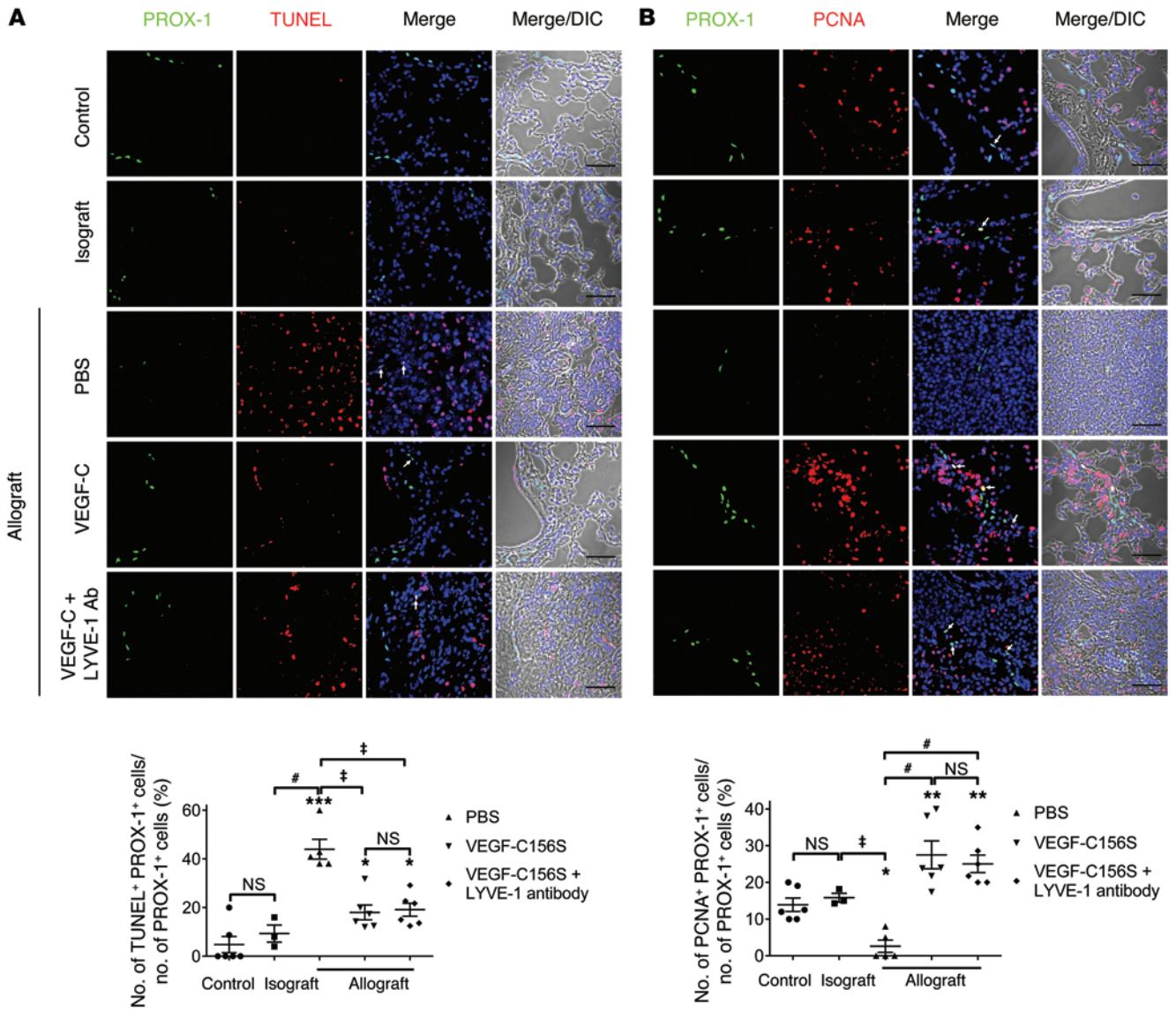

Figure 4. VEGF-C156S treatment ameliorates LEC apoptosis and promotes LEC proliferation in lung allografts. (**A**) Upper panel: representative images of PROX-1 (green) and TUNEL (red) double immunofluorescence staining. PROX-1/TUNEL–double-positive cells are indicated by white arrows. Lower panel: percentage of TUNEL-positive LECs. (**B**) Upper panel: representative images of PROX-1 (green) and PCNA (red) double immunofluorescence staining. PROX-1/PCNA–double positive cells are indicated by white arrows. Lower panel: percentage of PCNA-positive LECs. Nuclei were counterstained with DAPI (blue). Scale bars: 50 μm (**A** and **B**). Animals receiving allogeneic lung grafts were treated with PBS (n = 5 mice) or VEGF-C156S (VEGF-C) (n = 6 mice) or were concomitantly treated with VEGF-C156S and LYVE-1 function–blocking antibody (VEGF-C + LYVE-1 Ab) (n = 6 mice) from day 20. Animals receiving isogeneic (n = 3 mice) or allogeneic lung grafts were sacrificed 30 days after transplantation, together with age-matched untransplanted controls (n = 6 mice). Data are presented as the mean ± SEM. $^{*}P < 0.05$, $^{**}P < 0.01$, $^{***}P < 0.001$ (versus control); $^{‡}P < 0.01$, $^{\#}P < 0.001$ (versus PBS-treated allografts). All P values were determined by 1-way ANOVA.

30 after transplantation were indistinguishable from those on day 20, indicating that the acute lung rejection observed on day 20 did not spontaneously regress. Coinciding with increased lymphangiogenesis, VEGF-C156S partially rescued the airspace consolidation within the allografts (aerated left lung volume increased by more than 14-fold), while blocking LYVE-1 nullified such therapeutic benefits (Figure 7B). Peak airway pressure (PawP) in the left lung was measured at the end of each study. Consistent with histology and μCT imaging observations, VEGF-C156S led to a decrease in PawP in allografts compared with PBS or VEGF-C156S plus LYVE-1 function-blocking antibody treatment (Figure 7C).

Decreased HA accumulation in treated human lung allografts correlates with improved functional outcome. To determine whether our findings in the animal model are consistent with acute rejection in human lung allografts, we analyzed lung tissue samples obtained from 5 lung transplant recipients diagnosed with acute rejection. Samples were obtained during routine surveillance transbronchial biopsies before and after treatment with high-dose methylprednisolone for 3 days, followed by a 2.5-week tapering of the prednisone dosage to the baseline. In agreement with the results from our preclinical studies, histologic resolution of acute rejection in these patients was accompanied by a marked decrease in HA

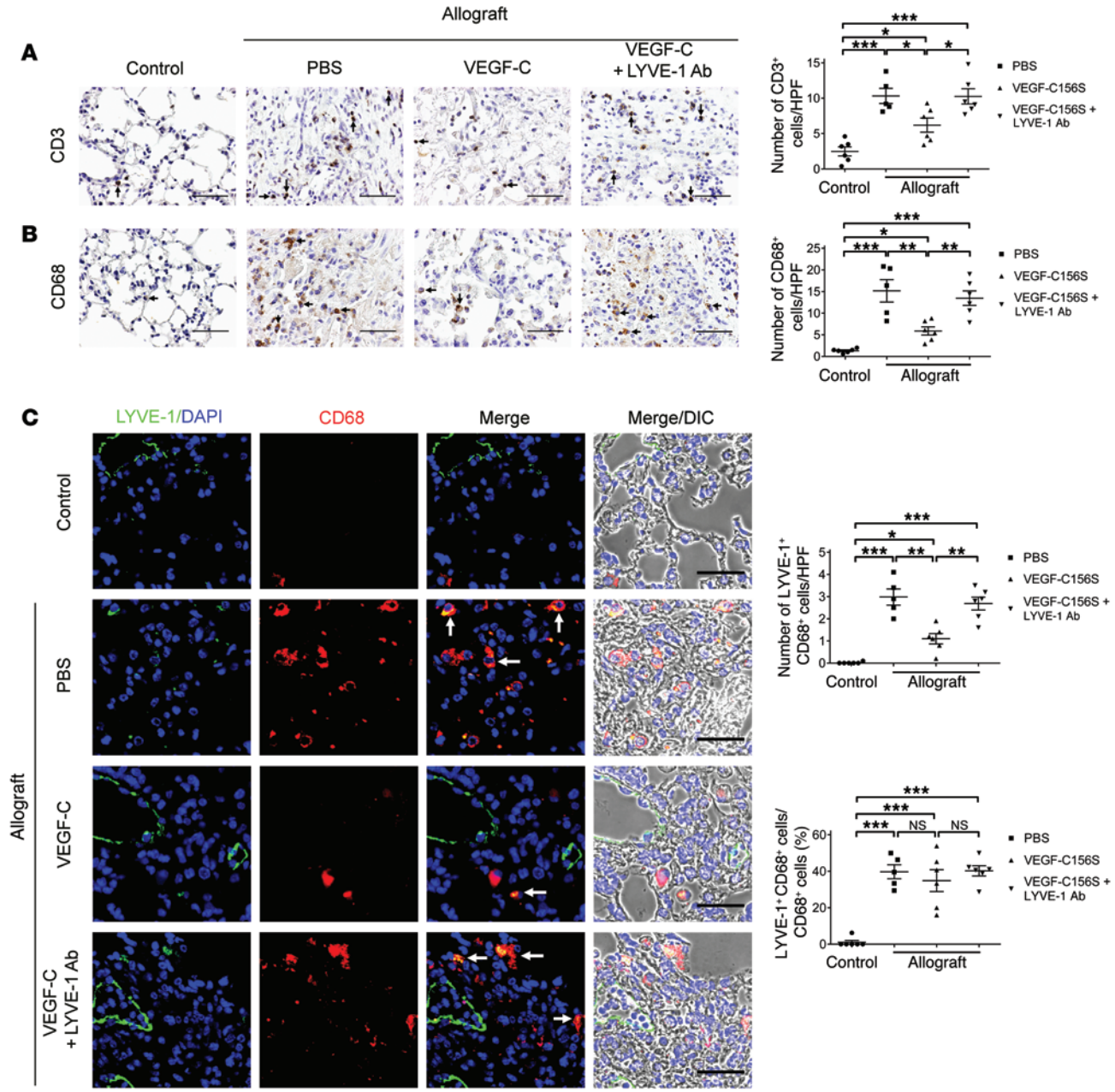

Figure 5. VEGF-C156S treatment reduces inflammatory cell infiltration into lung allografts. (**A** and **B**) Representative images of CD3 (**A**) and CD68 (**B**) immunohistochemical staining (black arrows, left panel) and quantification of positive cells per HPF (right panel). (**C**) Left panel: representative images of LYVE-1 (green)/CD68 (red) double immunofluorescence staining. LYVE-1/CD68–double-positive cells are indicated by white arrows. Nuclei were counterstained with DAPI (blue). Upper-right panel: quantification of LYVE-1/CD68–double-positive cells per HPF. Lower-right panel: percentage of LYVE-1–positive macrophages. Scale bars: 50 μm (**A** and **B**), 40 μm (**C**). Animals receiving allogeneic left lung grafts were treated with PBS (n = 5) or VEGF-C156S (VEGF-C) (n = 6) or with VEGF-C156S and LYVE-1 function–blocking antibody (VEGF-C + LYVE-1 Ab) (n = 6) from day 20 to day 30 after transplantation. Untransplanted animals were used as controls (n = 6). $^*P < 0.05$, $^{**}P < 0.01$, $^{***}P < 0.001$, as determined by 1-way ANOVA.

labeling in lung parenchyma (Figure 8A). Alleviation of rejection following high-dose corticosteroids was also confirmed by a pulmonary function test, which showed an increase in forced expiratory volume in 1 second (FEV1) compared with the baseline (Figure 8B). Interestingly, there was no significant difference in the density of podoplanin-positive (D2-40–positive, a specific human lymphatic vessel marker; refs. 53, 62) lymphatic vessels between the rejection and resolution stages (Figure 8C).

Discussion

In this study, we performed a comprehensive evaluation of lymphatic vessels in an orthotopic mouse lung transplant model and show that acute lung rejection leads to loss of pulmonary lymphatic vessels. Furthermore, we demonstrate that defective lymphatic drainage impairs clearance of HA fragments and results in aberrant HA accumulation, which has been previously associated with tissue injury (29, 30, 63) and the development of

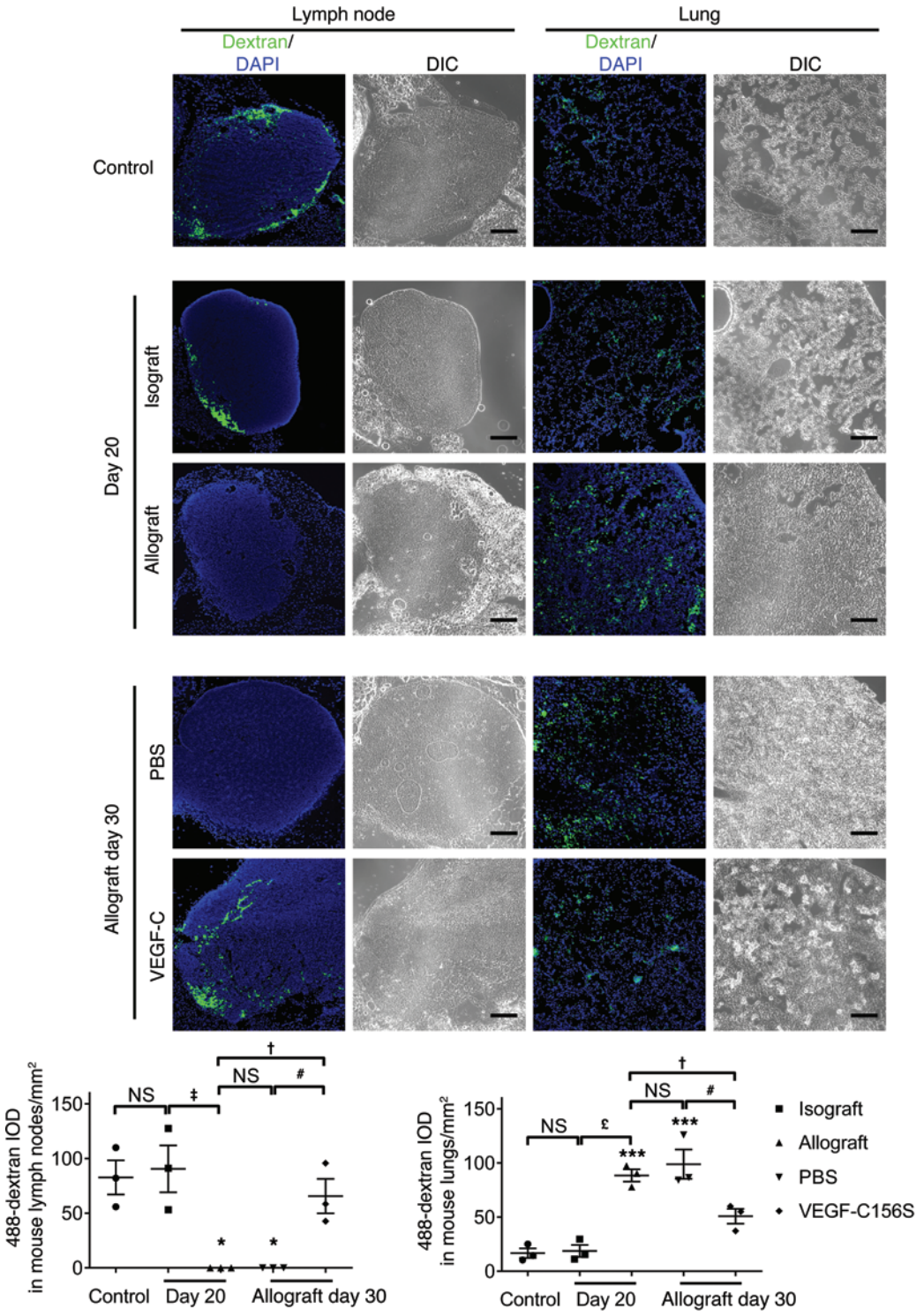

Figure 6. VEGF-C156S treatment restores lymphatic drainage in lung allografts. Representative images of 488-dextran in mouse left lungs and tracheobronchial lymph nodes (green, top panels) and quantification (bottom panels) of 488-dextran IOD. Tissues were collected 50 minutes after unilateral instillation of 488-dextran solution into mouse left lungs. A pulmonary 488-dextran drainage assay was performed in control mice, in animals receiving either isogeneic or allogeneic lung grafts on day 20 after transplantation (before treatment), and in allograft recipients treated with either PBS or VEGF-C156S (VEGF-C) from day 20 to day 30 after transplantation (n = 3 mice/group). Scale bars: 200 μm. Data are presented as the mean ± SEM. $^{*}P < 0.05$; $^{***}P < 0.001$ (versus control); $^{\dagger}P < 0.05$, $^{\ddagger}P < 0.01$, $^{£}P < 0.001$ (versus allografts on day 20); $^{\#}P < 0.05$ (versus allografts treated with PBS on day 30). All P values were determined by 1-way ANOVA.

BOS (33). Previous work has shown that modulating angiogenesis contributes to the long-term survival of tracheal allografts (7, 8). Here, we provide evidence that induction of therapeutic lymphangiogenesis mitigates established allograft rejection and is associated with augmented HA clearance. These findings underscore the importance of lymphatic vessels in lung transplants and suggest a missing link between HA transport abnormality and acute rejection.

Lymphatic vessels are instrumental in facilitating the transport of antigen-presenting cells (APCs) with allogeneic antigens to the draining lymph nodes (53, 64) and thus have been invariably associated with exacerbation of allograft rejection, particularly in the transplantation of avascular tissues such as cornea and cartilage (17, 18). In solid organ transplants, on the other hand, the regeneration of lymphatic vessels and restoration of lymphatic drainage are considered essential for maintaining postoperative tissue homeostasis and potentially beneficial for graft survival. For instance, human renal and heart allografts with a higher density of lymphatic vessels are less susceptible to severe forms of rejection (13, 15). In agreement with these clinical observations, our study provides experimental evidence to substantiate the importance of lymphatic drainage in graft survival and indicates that the absence of lymphatic vessels might be directly responsible for graft failure.

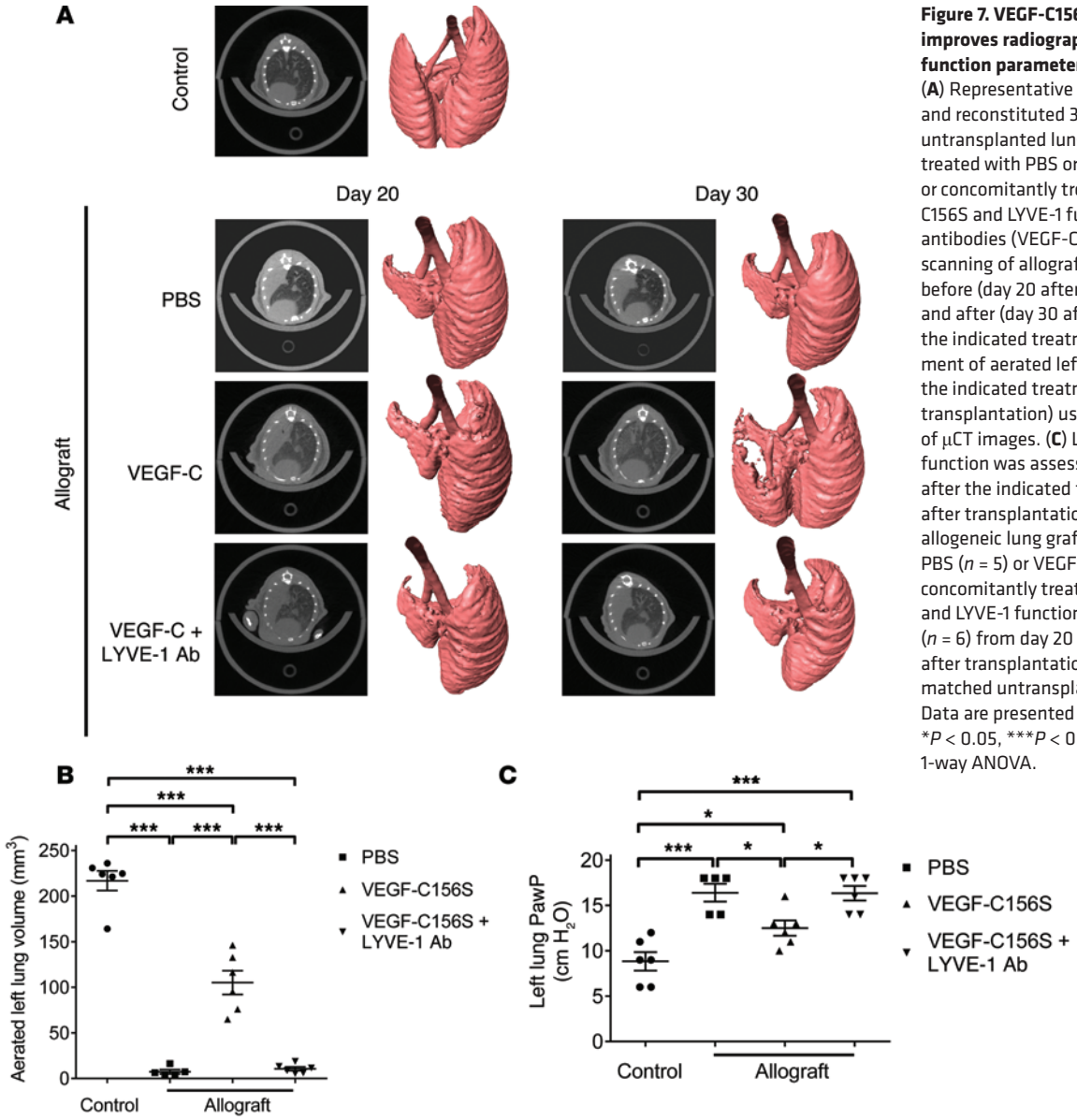

Figure 7. VEGF-C156S treatment improves radiographic and pulmonary function parameters in lung allografts. (**A**) Representative μCT axial slides and reconstituted 3D images of control untransplanted lungs and allografts treated with PBS or VEGF-C156S (VEGF-C) or concomitantly treated with VEGF-C156S and LYVE-1 function–blocking antibodies (VEGF-C + LYVE-1 Ab). μCT scanning of allografts was performed before (day 20 after transplantation) and after (day 30 after transplantation) the indicated treatment. (**B**) Measurement of aerated left lung volume after the indicated treatment (day 30 after transplantation) using 3D reconstruction of μCT images. (**C**) Left lung pulmonary function was assessed by PawP levels after the indicated treatment (day 30 after transplantation). Animals receiving allogeneic lung grafts were treated with PBS (n = 5) or VEGF-C156S (n = 6) or were concomitantly treated with VEGFC-156S and LYVE-1 function–blocking antibodies (n = 6) from day 20 and sacrificed 30 days after transplantation, together with age-matched untransplanted controls (n = 6). Data are presented as the mean ± SEM. $^*P < 0.05$, $^{***}P < 0.001$, as determined by 1-way ANOVA.

In addition to reabsorption of interstitial tissue fluid and trafficking of immune cells, lymphatic vessels maintain HA equilibrium by removing excessive HA degradation products through the endocytic receptor LYVE-1 (49). Experimental lung injury in different animal models is associated with increased HA content (30, 65, 66), although the accumulation of HA is only transient when the route of HA clearance is preserved (63). Our study highlights the importance of lymphatic transport in HA clearance during lung injury and suggests that the disappearance of functional lymphatic vessels could result in a pronounced accumulation of fragmented HA in rejected grafts. These findings strongly suggest deleterious effects of HA accumulation in lung transplants and provide evidence that lymphatic HA uptake affects graft outcomes (illustrated in Figure 9). We also present evidence that HA homeostasis in mouse untransplanted right lungs is not affected by LYVE-1 function–blocking antibodies. These findings are in line with published literature that shows a normal phenotype in the unchallenged *Lyve1*-KO mouse (67).

Previous studies suggest that apoptosis contributes to the development of allograft rejection (68, 69), although the occurrence of LEC apoptosis has not been documented. Here, we report that increased apoptosis and reduced proliferation are detected in pulmonary lymphatic endothelium within the allogeneic lung grafts undergoing acute rejection. The LECs originating from the donors display foreign antigens, which render these cells highly susceptible to the scrutiny of the recipient's immune system and, in particular, the injury inflicted by cytotoxic T cells (70). The changes we have witnessed in LEC apoptosis and proliferation could at least partially account for the overwhelming loss of lymphatic vessels in the rejected allografts observed in our study. It is also noteworthy that LEC apoptosis and proliferation in isografts were similar to what was seen in the control lungs, indicating that alterations of lymphatic vessels in lung allografts are most likely due to the initiation of alloimmune responses rather than to surgery-induced ischemia-reperfusion injury. Correspondingly, we show that VEGF-C156S rescues rejection-induced LEC apopto-

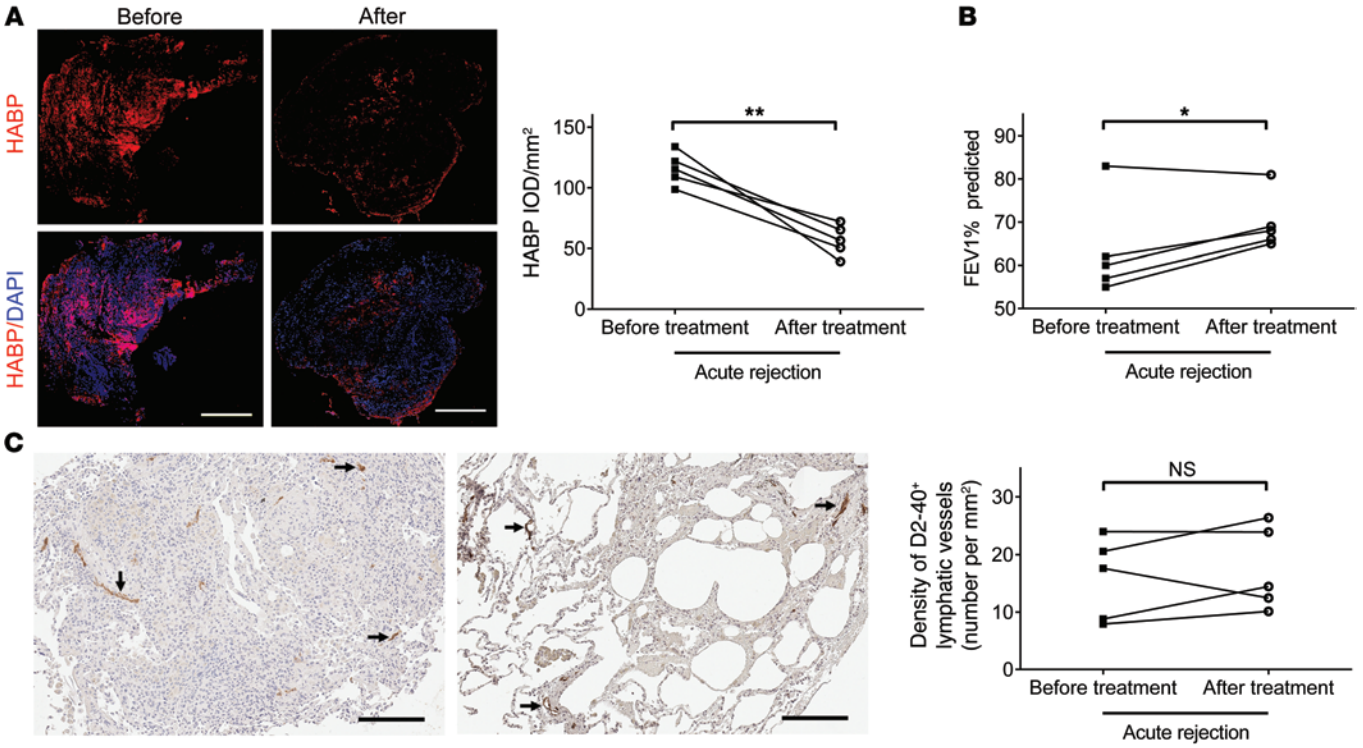

Figure 8. Decreased HA accumulation in treated human lung allografts correlates with improved functional outcome. (**A**) Left panel: representative images of paired HABP fluorescence staining (red) of human lung sections before and after treatment for acute lung rejection. Nuclei were counterstained with DAPI (blue). Right panel: quantification of HABP IOD. (**B**) FEV1 was measured before and after treatment for acute lung rejection. (**C**) Representative images of paired D2-40 immunostaining (indicated by black arrows) of human lung sections before and after treatment for acute lung rejection (left panels) and quantification of D2-40–positive lymphatic vessel density (right panel). Scale bars: 500 μm (**A**), 200 μm (**C**). $*P < 0.05$, $**P < 0.01$, as determined by paired 2-tailed Student's *t* test ($n = 5$ patients/group).

sis, induces LEC proliferation, restores lymphatic vessel density, and results in a functional lymphatic vasculature. Interestingly, emerging evidence suggests that, along with being the structural cells that form lymphatic vessels, LECs regulate T cell tolerance and suppress immunity (71–73). Therefore, we postulate that the preservation of intact LECs by inhibiting their apoptosis and inducing their proliferation is essential to modulate lung rejection.

As expected, we observed an inflammatory microenvironment in rejected allografts characterized by the aggregation of macrophages and T cells. Consistent with a previous report (45), treatment with VEGF-C156S blunted the inflammatory response. We also investigated whether the VEGF-C156S–driven improvement in HA clearance was dependent on other cell types, especially LYVE-1–positive macrophages recruited to the site of injury. Our data show that injury results in an increase in LYVE-1–positive macrophages, which is dampened by VEGF-C156S treatment and increased by concomitant blocking of LYVE-1 function. These data suggest that the recruitment of LYVE-1–positive macrophages is dependent on the injury and not the VEGF-C treatment. Further, the accumulation of LYVE-1–positive macrophages in injured lungs alone is not sufficient to clear HA in the absence of a functional lymphatic bed.

Of particular relevance to our study, a recent study using a rat heterotopic tracheal transplant model reported that an increase in the number of lymphatics is associated with the development of obliterative bronchiolitis (18). These contradictory observations may largely reflect the intrinsic biological differences between the animal models. Unlike human lung transplants, the tracheal transplant model utilizes an allograft that contains an avascular cartilaginous structure, which is neither aerated nor vascularized. On the other hand, the orthotopic mouse lung transplant model in the present study physiologically mimics vascularized aerated human lung allograft (74) and thereby offers an ideal platform to address the role of lymphangiogenesis in lung transplant. It is also noteworthy that in the tracheal transplant model, the increase in the number of lymphatic vessels in the cartilaginous structures of the airway wall is accompanied by a dramatic loss of subepithelial lymphatic vessels. Additionally, overexpression of exogenous VEGF-C prevents epithelium damage through the induction of lymphangiogenesis but exacerbates luminal occlusion of the tracheal allografts (18). These results suggest that the fate of lymphatic vessels in the noncartilaginous portion of the trachea (i.e., the element that bears the closest resemblance to human lung transplant) is similar to that in our model.

Unlike WT VEGF-C, VEGF-C156S possesses a point mutation that renders it selective toward VEGFR-3 but not VEGFR-2 (44). The unique feature of this mutant enabled us to avoid the induction of angiogenesis and determine the critical function of inducing lymphangiogenesis exclusively after lung transplantation surgery. Remarkably, previous reports suggest that concurrent activation of VEGFR-2 and VEGFR-3 by VEGF-C overexpression is associated with increased microvascular permeability and neutrophil infiltration (18), yet administration of VEGF-C156S inhibits inflammation

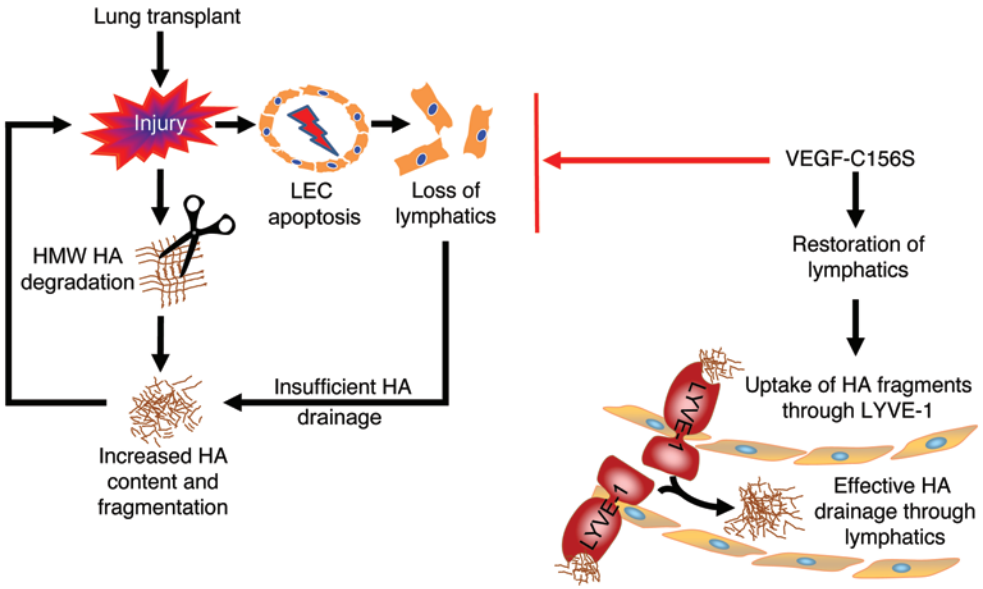

Figure 9. Schematic illustration of how lymphatic HA uptake affects graft outcomes. Acute lung rejection induces increased HA content and fragmentation. Meanwhile, LEC apoptosis during acute rejection leads to loss of pulmonary lymphatic vessels. The disappearance of pulmonary lymphatic vessels results in pronounced accumulation of fragmented HA, which in turn causes further damage to the graft. Conversely, stimulating lymphangiogenesis by therapeutic application of VEGF-C156S improves HA clearance by removing excessive HA degradation products through the endocytic receptor LYVE-1 in lymphatic endothelium and alleviates the rejection response.

without interfering with the blood vasculature (45). Thus, attempts to minimize unintended VEGF receptor binding in order to avoid disturbing blood vessel integrity could also be critical in future therapeutic endeavors to treat lung transplant rejection.

Our longitudinal assessment of transplant patients demonstrates that there is a dramatic reduction in HA deposition when acute lung rejection resolves with high-dose corticosteroids. Notably, pulmonary lymphatic vessel density is not significantly different between the rejection and resolution stages. This seemingly paradoxical observation suggests that factors other than lymphatic drainage contribute to the decrease of HA in these patients. Indeed, corticosteroids have been shown to exert a rapid and robust suppressive effect on HA synthases (HASs) by decreasing their mRNA production and stability (75, 76). Additionally, corticosteroids inhibit hyaluronidase production, resulting in a diminished presence of fragmented HA (77). It is worth noting that immunosuppression leads to disrupted lymphatic function (78) and, as a result, might compromise effective HA drainage. Such affects could potentially result in aberrant HA accumulation in the long term and thus put the patients at greater risk for recurrent acute lung rejection and BOS. In fact, more than half of lung transplant recipients still suffer from acute rejection and succumb to chronic rejection despite prophylactic immunosuppression (3, 4), indicating that immunosuppression alone might not be adequate for the successful management of lung transplant rejection in a subset of patients. Taken together, the cumulative findings of the present and previous studies (78) suggest that a combination of immunosuppression and prolymphangiogenic therapy that aims to maintain lymphatic vessels could be a therapeutic option for patients with acute lung rejection.

In conclusion, our findings add substantially to the understanding of lung transplant pathophysiology by linking the loss of lymphatic vessels to increased HA deposition in rejected allografts. We also provide evidence that stimulation of lymphangiogenesis attenuates established allograft lung rejection, likely through facilitating the clearance of HA degradation products. Our results establish lymphatic drainage as a critical determinant of lung transplant outcomes, and we propose that prolymphangiogenic therapy could be beneficial for long-term graft survival.

Methods

Orthotopic mouse lung transplantation. Male BALB/c and C57BL/6 mice, 10–12 weeks of age, were purchased from The Jackson Laboratory. Orthotopic left lung transplantations were performed as previously described (79, 80). Briefly, donor mice were anesthetized with an i.p. injection of ketamine/xylazine. They were intubated and connected to a small animal ventilator (Harvard Apparatus). A median laparosternotomy was performed, and heparin (100 units) was administered i.v. Afterwards, lungs were flushed, and the heart-lung block was harvested. The left lung was isolated, and cuffs were placed on the pulmonary artery, vein, and bronchus. Subsequently, recipient mice were anesthetized and mechanically ventilated. A left-sided thoracotomy in the third intercostal space was performed, and the recipient's left lung was gently retracted by a binder clip to expose the left hilum. The left pulmonary artery, vein, and bronchus of the recipients were then dissected free of adjacent tissue. Cuffed donor pulmonary artery, bronchus, and vein were inserted into corresponding recipient structures, and the anastomosis was secured with a 10-0 nylon tie. The recipient left lung was removed following implantation of the donor lung. Finally, the incision was closed in layers, and the animal was extubated.

Drug therapy. The following experimental groups were used: (a) Control untransplanted C57BL/6 mice; (b) C57BL/6 donor to C57BL/6 recipient (isografts); (c) BALB/c donor to C57BL/6 recipient (allografts); (d) allografts treated with PBS through i.v. injection; (e) allografts treated with VEGF-C156S (125 μg/kg per day) (R&D Systems) through i.v. injection; (f) allografts treated with VEGF-C156S (125 μg/kg per day) through i.v. injection in addition to LYVE-1 function–blocking antibodies (100 μg per animal every other day) (R&D Systems) administered by i.p. injection.

Mice were injected from day 20 after transplantation until sacrifice on day 30. The dose and route of administration of VEGF-C156S and LYVE-1 function–blocking antibody were chosen on the basis of preliminary experiments and published studies (50, 81).

CT imaging. In vivo imaging of mouse lungs was performed at the indicated time points using a MicroCAT II scanner (Siemens Preclinical Solutions) as previously described (79). Serial sections were subse-

quently imported into Amira software (Visualization Sciences Group) for segmentation and 3D surface rendering. In addition, segmentation of the left lung was performed in each transverse slice as previously described (82). The selected regions of interest (ROI) were then imported into VivoQuant software (inviCRO) for measurement of left lung volume.

Lung function. PawP of the left lung was measured at the end of each study to evaluate lung function, as previously described (38, 83, 84). Briefly, mice were intubated and mechanically ventilated under isoflurane anesthesia. Laparosternotomy was performed, and the right mainstem bronchus was temporarily occluded with a microvascular clip. PawP from the left lung was measured using a pressure transducer attached to a 3-way stopcock placed between the endotracheal tube and the ventilator.

Histology. The lower portion of the left lung was fixed in 10% formalin for 48 hours. Following formalin fixation, the lungs were paraffin embedded, sectioned into 5-μm slices, and stained with H&E. An experienced lung transplant pulmonologist (G. Visner) evaluated the severity of graft rejection in a blinded manner using the standard grading criteria established by the Lung Rejection Study Group of the International Society for Heart and Lung Transplantation (ISHLT) (85).

IHC and immunofluorescence. Tissue sections were deparaffinized in xylene and rehydrated through a graded series of ethanol solutions, followed by heat-induced epitope retrieval in citrate buffer (pH 6.0). Sections were blocked with normal serum and incubated with primary antibodies in a humidified chamber overnight at 4°C. A complete list of primary antibodies is provided in Supplemental Table 1. For IHC staining, sections were subsequently incubated with the appropriate secondary antibodies using an HRP-DAB Cell & Tissue Staining Kit (R&D Systems) according to the manufacturer's instructions. Finally, sections were briefly counterstained with hematoxylin. For immunofluorescence staining, sections were incubated with Alexa Fluor–conjugated secondary antibodies (Life Technologies) for 1 hour at room temperature in the dark. Slides were mounted using antifade mounting medium containing DAPI (Vector Laboratories). An isotype match was used in place of the primary antibody to verify the staining specificity.

LEC apoptosis was detected by TUNEL staining using the In Situ Cell Death Detection Kit, TMR red (Roche Applied Science) according to the manufacturer's recommendations. Sections were then stained with a PROX-1 antibody (R&D Systems), followed by Alexa Fluor–conjugated donkey anti-goat IgG (Life Technologies) to localize LECs. Positive (DNase I incubation) and negative (label solution only) controls of TUNEL staining as well as negative controls with nonimmune goat IgG were used to validate staining specificity.

HA staining in histological sections was performed using a biotinylated HA–binding protein (Seikagaku Ltd.) and Texas red dye–conjugated streptavidin (Jackson ImmunoResearch Laboratories Inc.) as previously described (62). In addition, hyaluronidase (Seikagaku Ltd.) pretreatment was applied to consecutive sections to confirm the specificity of HA staining.

HA size analysis. Pooled tissue samples ($n = 5–6$/group; total weight, 60 mg) from the upper portion of the left lung were subjected to HA measurement as previously described (86–88). Samples were digested with proteinase K and chondroitinase ABC (pH 7.0). HA molecular weight ladders (Hyalose LLC) and samples were loaded onto a 0.7% agarose gel and stained with Stain-All (Sigma-Aldrich) after electrophoresis. Images were acquired using a ChemiDoc XRS+ imaging system with Image Lab image acquisition software (Bio-Rad) and analyzed with Quantity One software (Bio-Rad).

Evaluation of pulmonary lymphatic drainage. A protocol to investigate lymphatic drainage of the left lung was modified from a previously published study (50). Mice were anesthetized with an i.p. injection of ketamine/xylazine and suspended on a rodent intubation stand with the upper incisors hooked over the incisor wire. Vocal folds were visualized with the aid of an otoscope (Hallowell EMC). Left main bronchus intubation was performed with a modified catheter using a previously described wire-guided technique (89). Dextran–Alexa Fluor 488 (40 μl) solution (5 μg/μl diluted in PBS; 10,000 MW; Life Technologies) was subsequently instilled into the left main bronchus through the catheter. The left lungs and tracheobronchial lymph nodes were collected 50 minutes after instillation. The lungs were inflated with a 1:1 mixture of Tissue-Tek OCT Compound (Sakura Finetek) and PBS. Samples were then embedded in Tissue-Tek OCT Compound and solidified on dry ice. Frozen 10-μm sections were cut using a cryostat (Leica Biosystems), mounted on positively charged slides, and fixed with 4% paraformaldehyde in PBS.

Surveillance transbronchial lung biopsies in post-transplantation patients. Recipients of lung transplants at Brigham and Women's Hospital underwent routine surveillance bronchoscopy with transbronchial biopsies. If acute cellular rejection was diagnosed, patients were treated with high-dose methylprednisolone (SOLU-MEDROL; Pfizer, 1 g i.v. daily) for 3 days, followed by a 2.5-week tapering of the prednisone dosage to the baseline. Bronchoscopy and TBB were performed 6 weeks later to confirm resolution of the acute rejection.

Microscopy and image analysis. Microscopic images were acquired with an Olympus FSX-100 microscope and an Olympus FV-10i confocal laser scanning microscope. Images were imported into ImageJ software, version 1.36b (NIH) or Image-Pro Plus software, version 6.0 (Media Cybernetics Inc.) for quantification. All digital images were acquired and analyzed in a blinded manner.

Multiple photomicrographs of LYVE-1, VEGFR-2, and D2-40 immunohistochemical staining and HA immunofluorescence staining were captured and aligned to generate panoramic images of entire tissue sections. The differentially immunostained lymphatic and blood vessels were outlined manually. Lymphatic and blood vessel density was expressed as the total number of lymphatic or blood vessels in the entire tissue, divided by the area of the entire tissue. Quantitative measurement of HA fluorescence intensity was performed, and the result was adjusted for total tissue area.

For VEGFR-3/PROX-1 double immunofluorescence staining, 25 images were randomly acquired per lung section for each animal. Guided by differential interference contrast (DIC) images, double-positive lymphatic vessels were identified and counted. The density was calculated by dividing the total number of double-positive lymphatic vessels by the total size of all 25 images. In addition, the percentage of PROX-1/VEGFR-3–double-positive cells in the identified lymphatic vessels was calculated. For TUNEL/PROX-1 and PCNA/PROX-1 double immunofluorescence staining, images of 20 to 25 PROX-1–positive cells were randomly obtained. TUNEL/PROX-1– and PCNA/PROX-1–positive cells were separately identified, and the total number of double-positive cells was divided by the total number of PROX-1–positive cells for normalization.

For CD3 and CD68 IHC staining, the number of positive cells per lung tissue was counted in 10 randomly selected high-powered fields (HPFs) using a ×40 objective lens. An average number of positive cells per HPF was subsequently calculated. For CD68/LYVE-1 double

immunofluorescence staining, dual-labeled cells were identified in 10 randomly selected HPFs (with a ×60 objective lens) per animal. An average number of double-positive cells per HPF was calculated, and the total number of double-positive cells was divided by the total number of CD68-positive cells for normalization.

For the pulmonary lymphatic drainage assay, micrographs of the tracheobronchial lymph node and 10 random microscopic fields of lung sections were captured per animal. Quantitative measurement of 488-dextran fluorescence intensity was performed, and the result was adjusted for tissue area.

Statistics. Data are presented as the mean ± SEM. For mouse transplantation experiments, multiple comparisons were evaluated by 1-way ANOVA, followed by Tukey's post-hoc test. For clinical studies, we conducted paired 2-tailed Student's *t* tests to assess longitudinal differences in pulmonary function, lymphatic density, and HA levels before and after high-dose corticosteroid treatment. Analyses were performed using GraphPad Prism 5.0 (GraphPad Software). A *P* value of less than 0.05 was considered significant.

Study approval. Tissue from TBBs manifesting acute lung rejection and sequential TBBs indicating an absence of acute rejection within the first post-transplantation year were analyzed ($n = 5$) under protocols approved by the IRB of Brigham and Women's Hospital (Partners IRB protocol 2013P000560).

All animal experimental procedures were approved by the IACUC of Boston Children's Hospital (protocol 10-12-1851R).

Acknowledgments

This work was supported by NIH grants R21 HL119902 (to S.El-Chemaly) and P01HL108801 (to M. Perrella). The authors thank Elizabeth Henske and Bruce Levy for their support and helpful advice. We are grateful to B. Ith and E. Snay for their excellent technical support.

Address correspondence to: Souheil El-Chemaly, Division of Pulmonary and Critical Care Medicine, Brigham and Women's Hospital, 75 Francis Street, Boston, Massachusetts 02115, USA. Phone: 617.732.6869; E-mail: sel-chemaly@partners.org.

1. Arcasoy SM, Kotloff RM. Lung transplantation. *N Engl J Med*. 1999;340(14):1081–1091.
2. Yusen RD, et al. Lung transplantation in the United States, 1999–2008. *Am J Transplant*. 2010;10(4 pt 2):1047–1068.
3. Trulock EP, et al. Registry of the International Society for Heart and Lung Transplantation: twenty-fourth official adult lung and heart-lung transplantation report — 2007. *J Heart Lung Transplant*. 2007;26(8):782–795.
4. Martinu T, Chen DF, Palmer SM. Acute rejection and humoral sensitization in lung transplant recipients. *Proc Am Thorac Soc*. 2009;6(1):54–65.
5. Khalifah AP, et al. Minimal acute rejection after lung transplantation: a risk for bronchiolitis obliterans syndrome. *Am J Transplant*. 2005;5(8):2022–2030.
6. Burton CM, et al. Acute cellular rejection is a risk factor for bronchiolitis obliterans syndrome independent of post-transplant baseline FEV1. *J Heart Lung Transplant*. 2009;28(9):888–893.
7. Babu AN, et al. Microvascular destruction identifies murine allografts that cannot be rescued from airway fibrosis. *J Clin Invest*. 2007;117(12):3774–3785.
8. Jiang X, et al. Adenovirus-mediated HIF-1α gene transfer promotes repair of mouse airway allograft microvasculature and attenuates chronic rejection. *J Clin Invest*. 2011;121(6):2336–2349.
9. Griffith BP, et al. Anastomotic pitfalls in lung transplantation. *J Thorac Cardiovasc Surg*. 1994;107(3):743–753.
10. Kerjaschki D. The lymphatic vasculature revisited. *J Clin Invest*. 2014;124(3):874–877.
11. Rockson SG. Lymphatics and the heart: the importance of visceral lymphatic function in health and disease. *Lymphat Res Biol*. 2007;5(1):1–2.
12. Ruggiero R, et al. Detection of canine allograft lung rejection by pulmonary lymphoscintigraphy. *J Thorac Cardiovasc Surg*. 1994;108(2):253–258.
13. Geissler HJ, et al. First year changes of myocardial lymphatic endothelial markers in heart transplant recipients. *Eur J Cardiothorac Surg*. 2006;29(5):767–771.
14. Soong TR, Pathak AP, Asano H, Fox-Talbot K, Baldwin WM. Lymphatic injury and regeneration in cardiac allografts. *Transplantation*. 2010;89(5):500–508.
15. Stuht S, et al. Lymphatic neoangiogenesis in human renal allografts: results from sequential protocol biopsies. *Am J Transplant*. 2007;7(2):377–384.
16. Dashkevich A, et al. Lymph angiogenesis after lung transplantation and relation to acute organ rejection in humans. *Ann Thorac Surg*. 2010;90(2):406–411.
17. Dietrich T, et al. Cutting edge: lymphatic vessels, not blood vessels, primarily mediate immune rejections after transplantation. *J Immunol*. 2010;184(2):535–539.
18. Krebs R, et al. Critical role of VEGF-C/VEGFR-3 signaling in innate and adaptive immune responses in experimental obliterative bronchiolitis. *Am J Pathol*. 2012;181(5):1607–1620.
19. Zheng Y, Lin H, Ling S. Clinicopathological correlation analysis of (lymph) angiogenesis and corneal graft rejection. *Mol Vis*. 2011; 17:1694–1700.
20. Alitalo K. The lymphatic vasculature in disease. *Nat Med*. 2011;17(11):1371–1380.
21. Kim H, Kataru RP, Koh GY. Inflammation-associated lymphangiogenesis: a double-edged sword? *J Clin Invest*. 2014;124(3):936–942.
22. Bizargity P, Liu K, Wang L, Hancock WW, Visner GA. Inhibitory effects of pirfenidone on dendritic cells and lung allograft rejection. *Transplantation*. 2012;94(2):114–122.
23. Iken K, et al. Indoleamine 2,3-dioxygenase and metabolites protect murine lung allografts and impair the calcium mobilization of T cells. *Am J Respir Cell Mol Biol*. 2012;47(4):405–416.
24. Krupnick AS, et al. Central memory $CD8^+$ T lymphocytes mediate lung allograft acceptance. *J Clin Invest*. 2014;124(3):1130–1143.
25. Yoshida S, Sekine Y, Saitoh Y, Yasufuku K, Iwata T, Fujisawa T. Surgical technique of experimental lung transplantation in rabbits. *Ann Thorac Cardiovasc Surg*. 2005;11(1):7–11.
26. Ruggiero R, et al. Detection of canine allograft lung rejection by pulmonary lymphoscintigraphy. *J Thorac Cardiovasc Surg*. 1994;108(2):253–258.
27. Ruggiero R, et al. Reestablishment of lymphatic drainage after canine lung transplantation. *J Thorac Cardiovasc Surg*. 1993;106(1):167–171.
28. Scheibner KA, Lutz MA, Boodoo S, Fenton MJ, Powell JD, Horton MR. Hyaluronan fragments act as an endogenous danger signal by engaging TLR2. *J Immunol*. 2006;177(2):1272–1281.
29. Jiang D, Liang J, Noble PW. Hyaluronan in tissue injury and repair. *Annu Rev Cell Dev Biol*. 2007;23:435–461.
30. Jiang D, et al. Regulation of lung injury and repair by Toll-like receptors and hyaluronan. *Nat Med*. 2005;11(11):1173–1179.
31. Jiang D, Liang J, Noble PW. Regulation of non-infectious lung injury, inflammation, and repair by the extracellular matrix glycosaminoglycan hyaluronan. *Anat Rec (Hoboken)*. 2010;293(6):982–985.
32. Tesar BM, Jiang D, Liang J, Palmer SM, Noble PW, Goldstein DR. The role of hyaluronan degradation products as innate alloimmune agonists. *Am J Transplant*. 2006;6(11):2622–2635.
33. Todd JL, et al. Hyaluronan contributes to bronchiolitis obliterans syndrome and stimulates lung allograft rejection through activation of innate immunity. *Am J Respir Crit Care Med*. 2014;189(5):556–566.
34. Hallgren R, Gerdin B, Tengblad A, Tufveson G. Accumulation of hyaluronan (hyaluronic acid) in myocardial interstitial tissue parallels development of transplantation edema in heart allografts in rats. *J Clin Invest*. 1990;85(3):668–673.
35. Knudson CB, Knudson W. Hyaluronan-binding proteins in development, tissue homeostasis, and disease. *FASEB J*. 1993;7(13):1233–1241.
36. Laurent TC, Fraser JR. Hyaluronan. *FASEB J*. 1992;6(7):2397–2404.
37. Krupnick AS, et al. Orthotopic mouse lung transplantation as experimental methodology to study transplant and tumor biology. *Nat Protoc*. 2009;4(1):86–93.
38. Liu K, et al. Inhibition of the purinergic pathway

prolongs mouse lung allograft survival. *Am J Respir Cell Mol Biol*. 2014;51(2):300–310.
39. Podgrabinska S, Braun P, Velasco P, Kloos B, Pepper MS, Skobe M. Molecular characterization of lymphatic endothelial cells. *Proc Natl Acad Sci U S A*. 2002;99(25):16069–16074.
40. Baluk P, McDonald DM. Markers for microscopic imaging of lymphangiogenesis and angiogenesis. *Ann N Y Acad Sci*. 2008;1131:1–12.
41. Baluk P, et al. Pathogenesis of persistent lymphatic vessel hyperplasia in chronic airway inflammation. *J Clin Invest*. 2005;115(2):247–257.
42. Kretschmer S, Dethlefsen I, Hagner-Benes S, Marsh LM, Garn H, Konig P. Visualization of intrapulmonary lymph vessels in healthy and inflamed murine lung using CD90/Thy-1 as a marker. *PLoS One*. 2013;8(2):e55201.
43. Mouta Carreira C, et al. LYVE-1 is not restricted to the lymph vessels: expression in normal liver blood sinusoids and down-regulation in human liver cancer and cirrhosis. *Cancer Res*. 2001;61(22):8079–8084.
44. Joukov V, et al. A recombinant mutant vascular endothelial growth factor-C that has lost vascular endothelial growth factor receptor-2 binding, activation, and vascular permeability activities. *J Biol Chem*. 1998;273(12):6599–6602.
45. Huggenberger R, Ullmann S, Proulx ST, Pytowski B, Alitalo K, Detmar M. Stimulation of lymphangiogenesis via VEGFR-3 inhibits chronic skin inflammation. *J Exp Med*. 2010;207(10):2255–2269.
46. Saaristo A, et al. Lymphangiogenic gene therapy with minimal blood vascular side effects. *J Exp Med*. 2002;196(6):719–730.
47. Zheng W, Aspelund A, Alitalo K. Lymphangiogenic factors, mechanisms, and applications. *J Clin Invest*. 2014;124(3):878–887.
48. Banerji S, et al. LYVE-1, a new homologue of the CD44 glycoprotein, is a lymph-specific receptor for hyaluronan. *J Cell Biol*. 1999;144(4):789–801.
49. Prevo R, Banerji S, Ferguson DJ, Clasper S, Jackson DG. Mouse LYVE-1 is an endocytic receptor for hyaluronan in lymphatic endothelium. *J Biol Chem*. 2001;276(22):19420–19430.
50. Meinecke AK, et al. Aberrant mural cell recruitment to lymphatic vessels and impaired lymphatic drainage in a murine model of pulmonary fibrosis. *Blood*. 2012;119(24):5931–5942.
51. Klotz L, et al. Cardiac lymphatics are heterogeneous in origin and respond to injury. *Nature*. 2015;522(7554):62–67.
52. Visuri MT, et al. VEGF-C and VEGF-C156S in the pro-lymphangiogenic growth factor therapy of lymphedema: a large animal study. *Angiogenesis*. 2015;18(3):313–326.
53. D'Alessio S, et al. VEGF-C-dependent stimulation of lymphatic function ameliorates experimental inflammatory bowel disease. *J Clin Invest*. 2014;124(9):3863–3878.
54. Fischer S, et al. Cell death in human lung transplantation: apoptosis induction in human lungs during ischemia and after transplantation. *Ann Surg*. 2000;231(3):424–431.
55. Song R, et al. Carbon monoxide induces cytoprotection in rat orthotopic lung transplantation via anti-inflammatory and anti-apoptotic effects. *Am J Pathol*. 2003;163(1):231–242.
56. Heckman CA, et al. The tyrosine kinase inhibitor cediranib blocks ligand-induced vascular endothelial growth factor receptor-3 activity and lymphangiogenesis. *Cancer Res*. 2008;68(12):4754–4762.
57. Veikkola T, et al. Intrinsic versus microenvironmental regulation of lymphatic endothelial cell phenotype and function. *FASEB J*. 2003;17(14):2006–2013.
58. Attout T, et al. Lymphatic vascularisation and involvement of Lyve-1+ macrophages in the human onchocerca nodule. *PLoS One*. 2009;4(12):e8234.
59. Cho CH, et al. Angiogenic role of LYVE-1-positive macrophages in adipose tissue. *Circ Res*. 2007;100(4):e47–e57.
60. Schledzewski K, et al. Lymphatic endothelium-specific hyaluronan receptor LYVE-1 is expressed by stabilin-1$^+$, F4/80$^+$, CD11b$^+$ macrophages in malignant tumours and wound healing tissue in vivo and in bone marrow cultures in vitro: implications for the assessment of lymphangiogenesis. *J Pathol*. 2006;209(1):67–77.
61. Saaristo A, et al. Vascular endothelial growth factor-C gene therapy restores lymphatic flow across incision wounds. *FASEB J*. 2004;18(14):1707–1709.
62. El-Chemaly S, et al. Abnormal lymphangiogenesis in idiopathic pulmonary fibrosis with insights into cellular and molecular mechanisms. *Proc Natl Acad Sci U S A*. 2009;106(10):3958–3963.
63. Teder P, et al. Resolution of lung inflammation by CD44. *Science*. 2002;296(5565):155–158.
64. Ruddle NH. Lymphatic vessels and tertiary lymphoid organs. *J Clin Invest*. 2014;124(3):953–959.
65. Bai KJ, et al. The role of hyaluronan synthase 3 in ventilator-induced lung injury. *Am J Respir Crit Care Med*. 2005;172(1):92–98.
66. Li Z, Potts-Kant EN, Garantziotis S, Foster WM, Hollingsworth JW. Hyaluronan signaling during ozone-induced lung injury requires TLR4, MyD88, and TIRAP. *PLoS One*. 2011;6(11):e27137.
67. Gale NW, et al. Normal lymphatic development and function in mice deficient for the lymphatic hyaluronan receptor LYVE-1. *Mol Cell Biol*. 2007;27(2):595–604.
68. Szabolcs M, et al. Apoptosis of cardiac myocytes during cardiac allograft rejection. *Circulation*. 1996;94(7):1665–1673.
69. Zavazava N, Kabelitz D. Alloreactivity and apoptosis in graft rejection and transplantation tolerance. *J Leukoc Biol*. 2000;68(2):167–174.
70. Thaunat O, Kerjaschki D, Nicoletti A. Is defective lymphatic drainage a trigger for lymphoid neogenesis? *Trends Immunol*. 2006;27(10):441–445.
71. Podgrabinska S, et al. Inflamed lymphatic endothelium suppresses dendritic cell maturation and function via Mac-1/ICAM-1-dependent mechanism. *J Immunol*. 2009;183(3):1767–1779.
72. Norder M, Gutierrez MG, Zicari S, Cervi E, Caruso A, Guzman CA. Lymph node-derived lymphatic endothelial cells express functional costimulatory molecules and impair dendritic cell-induced allogenic T-cell proliferation. *FASEB J*. 2012;26(7):2835–2846.
73. Card CM, Yu SS, Swartz MA. Emerging roles of lymphatic endothelium in regulating adaptive immunity. *J Clin Invest*. 2014;124(3):943–952.
74. Jungraithmayr W, Jang JH, Schrepfer S, Inci I, Weder W. Small animal models of experimental obliterative bronchiolitis. *AmJ Respir Cell Mol Biol*. 2013;48(6):675–84.
75. Zhang W, Watson CE, Liu C, Williams KJ, Werth VP. Glucocorticoids induce a near-total suppression of hyaluronan synthase mRNA in dermal fibroblasts and in osteoblasts: a molecular mechanism contributing to organ atrophy. *Biochem J*. 2000;349(pt 1):91–97.
76. Kaback LA, Smith TJ. Expression of hyaluronan synthase messenger ribonucleic acids and their induction by interleukin-1beta in human orbital fibroblasts: potential insight into the molecular pathogenesis of thyroid-associated ophthalmopathy. *J Clin Endocrinol Metab*. 1999;84(11):4079–4084.
77. Papakonstantinou E, et al. Steroids and β2-agonists regulate hyaluronan metabolism in asthmatic airway smooth muscle cells. *Am J Respir Cell Mol Biol*. 2012;47(6):759–767.
78. Liao S, et al. Impaired lymphatic contraction associated with immunosuppression. *Proc Natl Acad Sci U S A*. 2011;108(46):18784–18789.
79. Liu K, et al. Inhibition of the purinergic pathway prolongs mouse lung allograft survival. *Am J Respir Cell Mol Biol*. 2014;51(2):300–310.
80. Jungraithmayr WM, Korom S, Hillinger S, Weder W. A mouse model of orthotopic, single-lung transplantation. *J Thorac Cardiovasc Surg*. 2009;137(2):486–491.
81. Bhansali SG, Balu-Iyer SV, Morris ME. Influence of route of administration and liposomal encapsulation on blood and lymph node exposure to the protein VEGF-C156S. *J Pharm Sci*. 2012;101(2):852–859.
82. Thiesse J, et al. Lung structure phenotype variation in inbred mouse strains revealed through in vivo micro-CT imaging. *J Appl Physiol (1985)*. 2010;109(6):1960–1968.
83. de Perrot M, et al. Recipient T cells mediate reperfusion injury after lung transplantation in the rat. *J Immunol*. 2003;171(10):4995–5002.
84. Liu H, Drew P, Gaugler AC, Cheng Y, Visner GA. Pirfenidone inhibits lung allograft fibrosis through L-arginine-arginase pathway. *Am J Transplant*. 2005;5(6):1256–1263.
85. Stewart S, et al. Revision of the 1996 working formulation for the standardization of nomenclature in the diagnosis of lung rejection. *J Heart Lung Transplant*. 2007;26(12):1229–1242.
86. Lee HG, Cowman MK. An agarose gel electrophoretic method for analysis of hyaluronan molecular weight distribution. *Anal Biochem*. 1994;219(2):278–287.
87. van der Windt GJ, et al. CD44 deficiency is associated with increased bacterial clearance but enhanced lung inflammation during Gram-negative pneumonia. *Am J Pathol*. 2010;177(5):2483–2494.
88. Forteza RM, Casalino-Matsuda SM, Falcon NS, Valencia Gattas M, Monzon ME. Hyaluronan and layilin mediate loss of airway epithelial barrier function induced by cigarette smoke by decreasing E-cadherin. *J Biol Chem*. 2012;287(50):42288–42298.
89. Singer T, et al. Left-sided mouse intubation: description and evaluation. *Exp Lung Res*. 2010;36(1):25–30.